THE JOURNAL OF PHYSICAL CHEMISTRY C

pubs.acs.org/JPCC Article

Push/Pull Effect as Driving Force for Different Optical Responses of Azobenzene in a Biological Environment

Stefan Knippenberg* and Silvio Osella*

Cite This: J. Phys. Chem. C 2020, 124, 8310–8322 Read Online

ACCESS | Metrics & More | Article Recommendations | Supporting Information

ABSTRACT: The specific relationship between the alkyl tail lengths of four azobenzene probes embedded in DOPC liquid disorder membrane and their (non) linear optical (NLO) properties have been considered in the current study. Using extensive molecular dynamics calculations, the push/pull effect of the alkyl tails on the position and orientation of the probes in the model membrane are discussed. The simulations indicate that with increasing tail lengths the cis isomers are pushed closer to the membrane surface, while the trans ones are rather pulled toward the membrane center. Throughout hybrid quantum mechanics/molecular mechanics calculations, the linear and nonlinear optical properties of these compounds have been investigated. The pushing effect of the tails for cis azobenzene is translated in strong responses in the (non) linear optical spectroscopies, while the opposite is seen for the trans isomers. The cis isomer can be seen as the active state of the azobenzene compound for membrane recognition. The current work highlights the correlation between the tails of photosensitive membrane probes and their NLO properties, and focuses on unexpected behaviors of azobenzene derivatives in biological environments which can be exploited in distinguishing between soft and stiff cellular compartments that are of utmost importance for ion carrier transport.

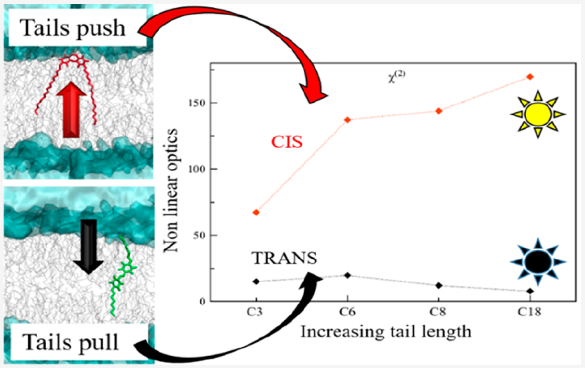

INTRODUCTION

A photoswitch is a molecule that undergoes a measurable and reversible change in its physical properties upon absorption of light, which can be viewed as an on/off switch with an "on" state in one form and an "off" state in the other form. One of the most widely known and used photoswitchable molecules is azobenzene, which undergoes geometric isomerization in the excited state from the stable trans to the metastable cis isomer. The advantage of azobenzene over other chromophores such as stilbenes lies in the fact that it does not undergo analogous irreversible closures to phenanthrenes, which makes azobenzene highly reversible.[1,2] The two isomers of azobenzene exhibit different absorption spectra; the cis azobenzene absorbs at a longer wavelength and can be selectively excited in the presence of the trans isomer.[3,4] With ultraviolet light, the trans azobenzene can be converted to the cis isomer, whereas with visible light (or heat) the process is reversed.[5] The interesting photophysics and photochemistry of this molecule induced a strong incentive for both experimentalists and theoreticians to design novel azobenzene-based materials whose functional properties such as volume, rigidity, and elasticity can be controlled by pulses of light.[6−9]

The azobenzene compound is a prototype for a molecular machine, which can be used as a building block to repetitively switch between two (meta)stable molecular states in a controlled manner. In particular, when bulk groups are connected to the benzene rings at the para position of the azo double bond, they can be moved closer together or further apart by applying light pulses, resulting in a switch between the cis and trans forms.[10] This idea can easily be exploited either in biology or material sciences; when a peptide is cyclized to an azobenzene, the subpicosecond photoisomerization of the chromophore, the dissipation of vibrational energy, and the subnanosecond conformational relaxation of the peptide can be observed by means of femtosecond time-resolved spectroscopy.[11] Polymers of azobenzenes have been lengthened and contracted by switching between trans and cis conformers, even against an external force acting along the polymer backbone, thus delivering mechanical work.[12] In all these designed optically active materials, the difference of ±2.4 Å between the end groups of the trans and cis conformers has been exploited.[13−19]

Trans/cis isomerization in biology can be used to transport ions across membranes if the conformationally versatile

Received: December 9, 2019
Revised: March 23, 2020
Published: March 26, 2020

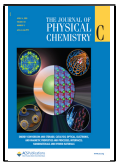

https://dx.doi.org/10.1021/acs.jpcc.9b11391
J. Phys. Chem. C 2020, 124, 8310–8322

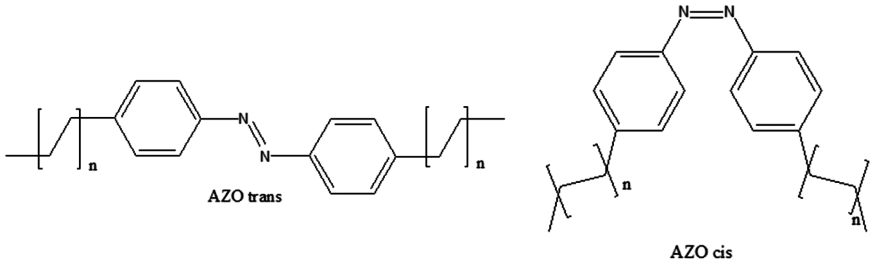

Figure 1. Chemical structures of the trans and cis azobenzene isomers considered in the study. n = 2, 5, 7, 17.

molecule permits a reversible and controllable binding of the cations, and if the chromophore can undergo reversible photoreactions.[20−22] With respect to antibiotic ion carriers, it is of utmost importance to take into account the membrane phase and the ease of the isomerization process in these environments, since steric hindrances and interactions with charged groups at the edges of the membrane depend on the conformation of the molecule. For biological systems, the azobenzene chromophore has an extra feature as its fluorescence anisotropy depends on the medium, which is found to affect the overall rotation and internal motions of the excited molecular probe.[23,24] Recently, we proved that the location and orientation of a cis azobenzene derivative in a liquid disordered membrane phase profoundly differs from the ones in a solid gel phase. This affected both linear and nonlinear optical properties of the compound as well as the fluorescence lifetimes of the isomers, making this probe an effective on/off switch for membrane recognition.[25] The knowledge of the membrane phase can be regarded as a key step in cancer research.[26] A depletion of cholesterol often characterizes cancer cells and induces a reduction of the fluidity or equivalently an increase in membrane order.[27] It is therefore not surprising that the potential of azobenzenes embedded in biological environments has been explored in the past decade. The photoswitching of azobenzene based micelles has been found to be highly reversible but can be suppressed in aggregates precipitated from the solution.[28] Azobenzene derivatives have been used as surfactants bound to DNA to induce and control conformational changes[29,30] to get insight into a stabilization of RNA and DNA hairpins.[31−33] Böckmann et al. developed an atomistic force field for a compound[34] which has been used to achieve photoisomerization driven peptide folding.[35−39] In literature, engineered biological pores responsive to external stimuli have been fruitfully used for various biotechnological applications, and azobenzene as a controlled artificial on/off switch has been found to provide a temporal control of designed nanodevices.[40−43]

Nonlinear optical techniques have been used to investigate many different chromophoric probes; it has been repeatedly proven that aromaticity emerges as an important concept in determining the photophysical properties and two-photon absorption cross sections of porphyrinoids,[44−49] which means that these compounds can be used for biomedical applications and photodynamic therapy as theranostic agents which have an excellent absorption in the biologically safe near-infrared region.[50] Moreover, conformational changes and conversions between open and closed forms of compounds like indolinooxazolidine derivatives can be used to induce enhancements of the first hyperpolarizability and to create molecular switches, which also can be used in optical memories.[51,52] From the biological point of view, giant unilamellar vesicles (GUVs) made of phospholipid molecules in which the photosensitive part of the molecule is embedded in the hydrophobic center of the molecule have been built with at least one of the acyl chains functionalized with an azobenzene group.[53] Lipid bilayer membranes and vesicles which are entirely composed of photoswitchable lipids can be deformed and bended reversibly by optical light and can be used to store energy which is released as locally usable work.[54]

In the current study, we focus on the influence of the varying lengths of four symmetric alkyl tails (composed of 3, 6, 8 and 18 carbon atoms, respectively, see Figure 1) on the position, location, and orientation of the trans and cis isomers of azobenzene embedded in a DOPC (dioleoylphosphatidylcholine) liquid disordered lipid bilayer membranes, which are found in red blood cells, in lung and in vein endothelial cells. Its alkyl tails are found to be essential for the push/pull effect they play on the position, orientation, and in the last instance on the response to optical properties of the two azobenzene isomers. The photoactivity of the azobenzene probes has been investigated by means of hybrid quantum mechanics−molecular mechanics calculations, which is indispensable as it has been proven that the immediate environment of the probe plays an important role in determining its linear and nonlinear spectra.[55] Thus, the study is extended toward the optical properties of the probe experimentally accessible, such as one- and two-photon absorption spectra, as well as the static component of the first and second hyperpolarizabilities β and γ, which give rise to the electric field-induced second harmonic generation (EFISHG). The complementarity of the techniques can be highlighted as the polarizability or linear absorption is dependent on the oscillator strength, while the hyperpolarizabilities are proportional to the difference in dipole moments between ground and excited states. Especially for the spectroscopies which depend on β, both the electronic features and the symmetry of the chromophore are important: the first one is responsible for the magnitude of the individual tensor components, while the symmetry determines which tensor components are zero and do not contribute to the overall signal.[56]

METHODS

The presented molecular dynamics (MD) calculations have been performed by means of the 43A1-S3 GROMOS force field[57,58] and the Gromacs 5.0.4 package of programs.[59−62] The methodology used through the study has been implemented and tested over different probes in different lipid membrane phases in our recent works on Laurdan, DiI, and azobenzene derivatives, and the conditions used here are the same as the ones reported in our previous works.[25,55,63−65] Parameters for the azobenzene headgroup have been taken from literature and are reported in Table S1 of the Supporting Information.[34] Briefly, at the onset of the equilibration the probe has been

https://dx.doi.org/10.1021/acs.jpcc.9b11391
J. Phys. Chem. C 2020, 124, 8310−8322

positioned in the water solvent with the long axis parallel to the membrane surface and in less than 30 ns penetrates the membrane. A 500 ns long molecular dynamics simulation has been performed in the canonical NPT ensemble at 323 K using the Nosé−Hoover thermostat[66,67] (with a time constant of 0.5 ps) and the Parrinello−Rahman barostat[68] (1 bar with a time constant of 2 ps and a compressibility of 4.5×10^{-5} bar^{-1}). The Particle Mesh Ewald (PME)[69] method was used to compute Coulomb and van der Waals interactions within a 1.2 nm cutoff; LINCS constrains have been used and the time integration step was set to 2 fs. Since it is known that the thickness of the DOPC membrane decreases at elevated temperatures as the swelling of the bilayer diminishes,[70] the study has been performed with a temperature of 323 K. The membrane and probe were solvated with water, using TIP3P parameters. The box size was set to $6.28 \times 6.10 \times 7.9$ nm, and the membrane surface has been oriented to be parallel to the *xy* plane. The MD simulations were considered equilibrated when the orientation of the transition dipole moment of the probe was found stable in the membrane; for this reason, for all the MD analysis we considered the 200−500 ns time window for each of the compounds. The partial charges on the probes have been derived from the electrostatic potential (ESP) scheme[71] as present in the Gaussian09 suite of programs[72] considering the CAM-B3LYP functional[73] and Dunning's cc-pVDZ basis set.[74]

From the eight different MD simulations (one per tail length and isomer) and each time focusing on the respective 200−500 ns time windows, 50 independent snapshots were extracted with a cylindrical cutoff of 10 nm for the membrane molecules surrounding the probe and a hemispherical cutoff of 1.5 nm for the water molecules in close contact with the membrane surface. The snapshots were used as an input for extensive hybrid quantum mechanical/molecular mechanics (QM/MM) calculations in which the probe (with its tails) was considered at the QM level of theory and the environment (i.e., lipid membrane and water molecules) was taken into account by means of point charges, as described at the MM level. The Dalton2016 program has been for this part of the work along with, again, the CAM-B3LYP functional and the cc-pVDZ basis set.[75] To evaluate the dependence of the nonlinear optical properties on the quality of the basis set, the TPA spectra for CC3 have been calculated also with the aug-cc-pVDZ basis set. As reported in the Supporting Information, the effect of the larger basis set on the TPA cross section is overall very limited.

The one-photon absorption spectra (OPA) of all the systems were analyzed and attention was paid to the nonlinear optical properties, such as two-photon absorption (TPA), and second harmonic generation phenomena. As reported in our previous studies,[25,55,64,76] the two-photon absorption cross section (in GM units) is computed as[77]

$$\sigma(\omega)_{GM} = \frac{8\pi^2\alpha^2 a_0^4 t_0}{\Gamma}\delta(\omega)\left(\frac{\omega}{2}\right)^2 \quad (1)$$

where α is the fine structure constant, a_0 is the Bohr radius, t_0 is the atomic unit for time, Γ is the Lorentzian broadening (considered a constant with a value of 0.1 eV), ω is the OPA excitation energy, and δ is the TPA strength in au.

The electric-field-induced second harmonic generation (EFISH) technique is a third-order process characterized by a nonlinear polarization $P^{2\omega}$. In the presence of an optical field parallel to the applied static electric field, the electric-field-dependent susceptibility is reduced to[78−80]

$$\chi^{(2)}(E^0) \sim \left(\langle\gamma\rangle + \frac{\bar{\beta}\cdot\bar{\mu}}{5kT}\right)E_0 \quad (2)$$

where $\langle\gamma\rangle$ is the orientationally averaged second hyperpolarizability and β is the static component of the first hyperpolarizability. It can be remarked that the second harmonic generation techniques can only be applied on noncentrosymmetric molecules. In the context of the current study, the azobenzene probes are embedded in anisotropic lipid bilayers at finite pressures and temperatures, which break the symmetry.

The scalar product $(\bar{\beta}\cdot\bar{\mu})$, denoted as β_{vec}, defines the vector component projected onto the ground state dipole moment

$$(\bar{\beta}\cdot\bar{\mu}) = \frac{1}{3}\sum_{i,j}(2\beta_{iij}\mu_j + \beta_{ijj}\mu_i) \quad (3)$$

A second experimental observable related to the hyperpolarizability β is the Hyper-Rayleigh Scattering (HRS). This scattering signal, independent from the dipole moment and the molecular symmetry, is measured by unpolarized optical excitation and can be derived as $\langle\beta_{HRS}\rangle = \sqrt{\langle\beta_{ZZZ}^2\rangle + \langle\beta_{XZZ}^2\rangle}$, where the brackets denote the orientational distribution average of the molecule in the environment and can be expressed as a combination of β_{ijk} tensor components in the frame of their molecular coordinates.[81]

To get insight into the electric-field-dependent susceptibility for the four cis and trans isomers of azobenzene, in this study we also assess the value of $\langle\gamma\rangle$, which can be computed using the molecular excited-state properties following an extended sum-overstate (SOS) approach.[82] For many π-conjugated molecules, the full expression can be simplified if a low-lying excited state is significantly coupled to the ground state. When the state dipole moments along the molecular long axis are large, the essential-state model can be used.[83,84] The full expression is given in Supporting Information and comprises 3 terms:[85] the dipole term which is proportional to $\mu_{ge}^2\Delta\mu_{eg}^2$; a two-photon term proportional to a sum of $\mu_{ge}^2\mu_{ee'}^2$ of overall higher excited states e′, and a negative term proportional to μ_{ge}^4. In the present work, μ_{ge} denotes the transition dipole moment between the ground state and the second excited state *e*. $\mu_{ee'}$ is the transition dipole moment between the second excited state and a higher lying excited state e′. $\Delta\mu_{eg}$ is the difference in state dipole moments between the second excited state and the ground state.

In fact, the same idea can also be expressed to the first hyperpolarizability. The dipolar term is here proportional to $\mu_{ge}^2\Delta\mu_{ge}$ (see also Supporting Information).

RESULTS AND DISCUSSION

MD Analyses. The effect of different tail lengths on the orientation and position of the azobenzene probe into the DOPC membrane is clearly visible from MD simulations. In particular, when we compare the position of the probes in the membrane (considered along the normal to the DOPC surface, in the specific case corresponding to the *z*-axis), we observe two distinct behaviors depending on the isomer considered. Figure 2 reports the density of the probes with different tails, the DOPC membrane and the phosphor atom, as representative of the membrane surface limit. To avoid confusion, throughout the study the probes are labeled as follows: trans isomer with 3, 6, 8, and 18 carbon atoms alkyl tails TC3, TC6, TC8, and TC18, respectively; cis isomer follows as CC3, CC6, CC8, and CC18. We would like to stress here that during the MD simulations

https://dx.doi.org/10.1021/acs.jpcc.9b11391
J. Phys. Chem. C 2020, 124, 8310−8322

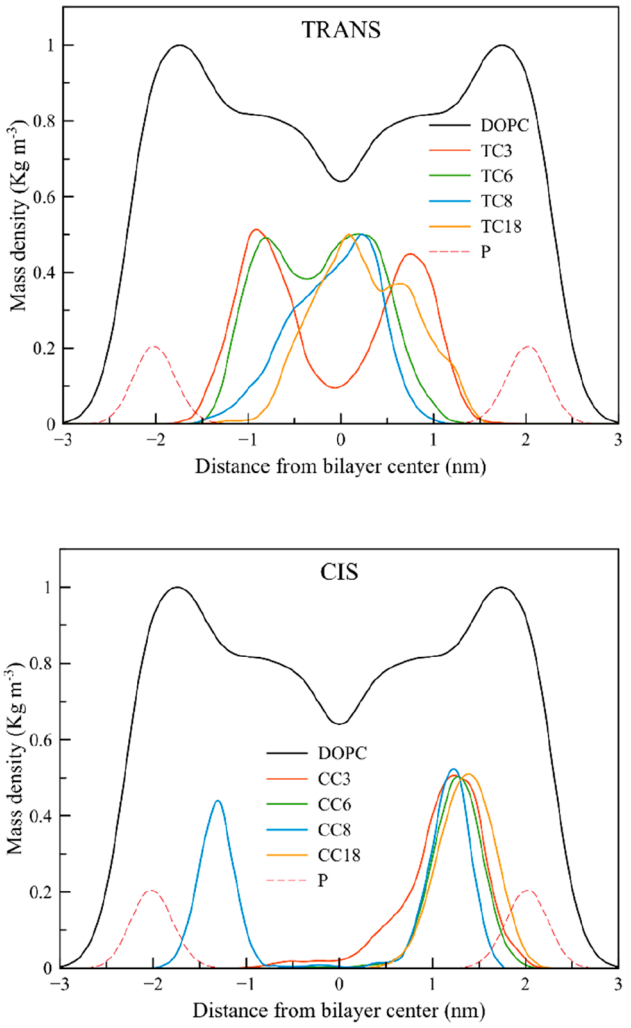

Figure 2. Mass density profile along the *z*-axis for the different components of the simulated box for the trans (top) and cis (bottom) isomers: DOPC (black), N═N probe position with three (red), six (green), eight (cyan), and eighteen (orange) carbon alkyl tails, and the phosphorus atoms of the membrane head (brown, dotted lines) are reported. The bilayer center is set at zero.

there is no switching between isomers (see Figure S1 in Supporting Information). For the density analysis, the N═N group is considered as representative position of the probes' core, that is, azobenzene without alkyl tails. Corresponding with the classification of Marrink and Berendsen, different regions are identified in a lipid bilayer membrane.[86] They are characterized by (1) a low headgroup density (at a distance of more than ∼2.40 nm from the membrane center), (2) a high headgroup density (between 2.40 and 1.25 nm), (3) a high tail density (between 1.25 and 0.50 nm), and (4) a low tail density (below 0.50 nm).

Already from this first analysis it is possible to observe the different effects of the tail lengths on the two azobenzene isomers. For trans, there is a constant drift toward the center of the lipid bilayer while increasing the tails length; the cis isomer is apparently unaffected by it and it is located at the same position, close to the membrane surface. In particular, for the trans isomer we measured a decreasing distance from the bilayer center of 0.83 nm for TC3, 0.38 for TC6, 0.23 nm for TC8 and 0.22 nm for TC18. The trans isomers are therefore all located in the high tail density region. For the more polar cis isomers, this is different as the high headgroup density region with its locally charged groups is reached: CC3, CC6, and CC8 are found at a constant value of 1.30 nm and CC18 is even seen slightly higher at 1.50 nm. It is already clear the effect of the tail lengths on the position of the probe. In fact, for the weakly polar trans isomer the tails tend to pull the azo-core toward the bilayer center as the lipophilic interactions in this region are more important than the hydrophilic ones; for the cis isomer the tails push the azo-core further closer to the membrane surface. A closer inspection of the position of the tails reveals that while for the cis isomer they are pointing toward the bilayer center irrespective of the length, for the trans the pulling effect is strongly correlated to the tail length, which in the final instance is the driving force for the particular, counterintuitive orientation of this isomer (density plots focusing on the different tail lengths are reported in Figure S2). This push/pull effect of the tails eventually affects also the stability of the conformer; in fact, while the cis isomer has opportunity to interact with the polar part of the membrane via the lone pair on the nitrogen atoms (which is included in the HOMO orbital, Figure S3), the trans isomer experiences a strong confinement in the bilayer apolar region due to the increased tails length, forcing it deeper into the membrane center. We see as well that for TC6, TC8, and TC18 one tail is embedded in the opposite leaflet. Together with the hydrophobicity of the tails, this explains the pulling effect. This is significant, since the membrane considered is in a liquid disordered phase which, in principle, should allow a high degree of motion of the tails, but the combination of the push/pull effects of the tails, their lengths, and the steric hindrance forbids a more parallel orientation of the trans isomer to the membrane surface. In addition, if we compare the TC3 and CC3 isomers, we observe that even with the shortest tail lengths the trans isomer is already located much deeper into the bilayer compared to the cis, which is very close to the membrane surface (calculated in respect to the phosphor atoms peak, at 2.20 nm and in excellent agreement with the experimental[70] literature value of 2.1 nm), once more pointing at the strong driving force arising from the tails' effect. Moreover, the position of the phenyl rings is also considered for the cis isomer, to shed light into the specific position of the probe as a whole (see Figure S4). It is interesting to notice that there is a high degree of symmetry in between the position of the two phenyl rings for all isomers. In fact, not only is the position retained but also the shape of the peaks is very similar with differences in position smaller than 0.5 nm for CC3, CC6, and CC8 and 0.1 nm for CC18. This can be explained considering once more the tail lengths; when longer tails are present, the probe is more confined in its position. It is a balance between the interaction of the azo core with the polar part of the membrane and the push-back of the tails from the lipophilic part which impedes the expected flexibility. The shorter CC3 tails have more freedom of movement, and as a consequence the phenyl rings also experience less steric hindrance. Yet, this situation does not affect the position of the phenyl rings with all of them peaking at around 1.24 nm from the bilayer center, while the azo group peak at 1.30 nm, confirming an orientation in which a lone pair interaction with the polar head of the membrane is favorable. Representative trans/cis structures are reported in Figure S5.

To further assess the differences arising from the different tail lengths, we analyzed the orientation of the probes, considering the angle formed between the transition dipole moment (tdm) and the normal to the membrane. It is possible to identify the tdm as a vector lying along the carbon atoms in para position of

https://dx.doi.org/10.1021/acs.jpcc.9b11391
J. Phys. Chem. C 2020, 124, 8310−8322

the phenyl groups for the trans isomer and along the azo group for the cis isomer (see insets in Figure 3).

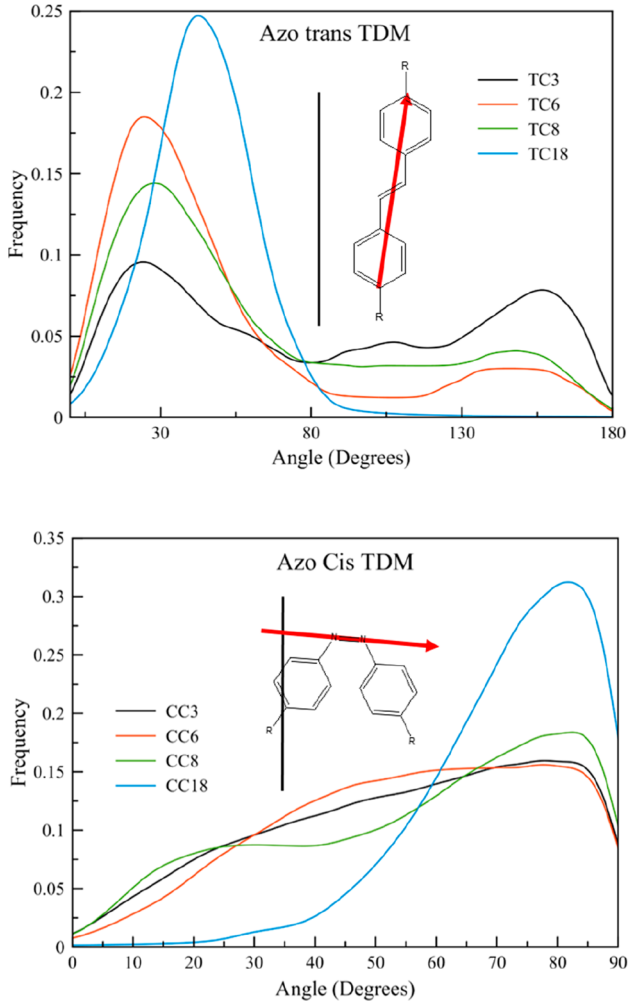

Figure 3. Distribution of the angle between the transition dipole moment of the probe and the normal to the membrane surface for both trans and cis isomers. The insets show a representation of the vectors used to compute the angles: red arrow refers to the tdm, the black line to the bilayer normal. Values for the cis isomer are reduced to the first quadrant.

Once more, the analysis confirms our previous finding; the TC3, TC6, and TC8 isomers present a very similar angle distribution with a main peak at around 25°, while TC18 is more tilted with a maximum angle of 43°. Moreover, TC3 presents a double, complementary distribution of angles which disappear while increasing the tail lengths. The different orientation obtained for TC18 can be directly linked to the fact that being located deep into the lipophilic part of the membrane, the azo-core tends to orient along with the surrounding membrane tails. This directly translates into a more tilted orientation of the whole probe to the normal of the bilayer. Especially for TC18, the probe's core is close to the membrane center and its movement is mainly determined by the first methylene groups of the tails. It can be remarked that the distributions of the angle of the transition dipole moment with the membrane normal ought to be symmetric around 90°. Any deviation can then be ascribed to the practical limitations of the computational time. For the trans isomers, we decided to show the complete picture in Figure 3 since it illustrates how the time scale becomes more and more restrictive with the length of the tails: for TC3, the curve is still symmetric, while for TC18 seemingly one side is preferred. This is due to fluctuations in the first few time steps of the systems. For TC3, the interactive forces of the tails with the lipids are rather limited and can be compensated at short time scales by the interactions which take place at finite temperature. However, for TC6 and TC8 the pulling effect of the tails increase and the sampling of the complete phase space becomes restricted.

CC3, CC6, and CC8 present a more perpendicular orientation to the bilayer normal with confined value of 80° for a flat plateau in between 60 and 80° for CC6 and a double feature at 20 and 80° appearing for CC8. Moreover, CC18 presents a sharper peak in which this plateau disappears, suggesting that the long tails force the orientation of the azo-core and decrease the wobbling of the molecule. This, together with a stronger dipole moment present for the cis isomer, directly translates into an almost perpendicular orientation of the whole probe to the normal bilayer, confirming the different push/pull effects of the tails on the two isomers. Interestingly, a similar behavior has been obtained for azobenzene-based polymers, where the cis isomer was found to be closer to the water interface due to the stronger dipole moment,[87] as well as in Langmuir–Blodgett films in which completely different orientations were measured for the trans (perpendicular) and the cis (parallel) isomers on the surface.[87]

To avoid the presence of artifacts due to the position of the azo group, an additional analysis on the orientation of the two phenyl rings of the azobenzene (the angle between the bilayer normal and the normal to the phenyl rings) has been performed, as reported in Figure S6. This last analysis confirms our previous results, as the orientation of the short-tailed trans isomer is only slightly tilted with respect to the bilayer normal. Through the simulations, the normal to the phenyl groups describe an angle of 90°, which arises from the strong hindrance of motion caused by the presence of the alkyl tails, and the consequent confinement of the aromatic core of the probe in close proximity to the bilayer center. For TC18, the high degree of flexibility of the tails and the stronger pull effect lead to a broader distribution of the phenyl groups, which might strongly deviate from a perpendicular one and allow a more tilted orientation.

The higher degree of flexibility present for the cis isomer is also indicated in this last analysis in which the orientation of the phenyl rings is more complex. To a different extent for all tail lengths, both rings present a peak at around 80–90° and a shoulder at around 125–140°. This translates into a dynamic exchange: one phenyl ring is oriented mainly parallel to the bilayer normal, while the second one is strongly tilted.

Finally, the photoselection for fluorescence experiments is discussed. This quantity depends on the angle θ between the field vector of the incoming beam and the orientation of the relevant transition state dipole moment through a $\cos^2\theta$ dependence (see Lakowicz[88] and references therein). In the current work, we assume that the incoming beam has a polarization along the membrane normal. The results for the four cis and trans isomers are expressed through an ensemble average and are given in Table 1. Considering 300 frames (in the 200–500 ns range), the results are found to be independent of the step size, which is chosen to be 1 ns. Despite the relatively high standard deviation, the table shows that photoselection is almost twice as probable for the trans azobenzene compounds rather than for the cis ones. This difference between the isomers can already be exploited in membrane research and enables

https://dx.doi.org/10.1021/acs.jpcc.9b11391
J. Phys. Chem. C 2020, 124, 8310–8322

Table 1. Efficiency of the Photoselection of the Four Cis and Trans Isomers in Fluorescence microscopy[ab]

TC3	TC6	TC8	TC18
0.56 (±0.33)	0.68 (±0.26)	0.57 (±0.31)	0.51 (±0.23)
CC3	CC6	CC8	CC18
0.32 (±0.32)	0.34 (±0.30)	0.35 (±0.33)	0.12 (±0.15)

[a]Calculated through $\langle \cos^2 \theta \rangle$ with θ as the angle of the transition dipole moment with respect to the membrane normal. [b]The brackets $\langle\ \rangle$ denote an average over the simulation time. The standard deviation is given in parentheses. The field vector of the incoming light beam is here assumed parallel to the normal of the membrane.

phase recognition by using optical techniques. The value for CC18 is considerably lower than for the other cis conformers and is a clear consequence of the peak at 80° in Figure 3. In addition, CC18 does only have a marginal population for the lower tilt angles, which affects the ensemble average.

In summary, the large difference in position and orientation of the two isomers affects the photoselection and is triggered by the push/pull effect due to the different tail lengths. It will be reflected as well by a different distribution of the surrounding solvent molecules and should have a tremendous impact on the optical response of the probes, allowing for the presence of on/off states.

2. Solvent Distribution. Since the cis conformers are positioned higher in the membrane with respect to the trans ones and thanks to the nature of the DOPC lipids in a liquid disordered membrane which allows water molecules to penetrate the membrane, it is expected that the amount of surrounding water molecules is also different in close proximity of both probes. As the trans isomers are located deeper into the membrane bilayer, the analysis focuses only on the cis isomers. Figure 4 shows that the cumulative solvent distribution is high

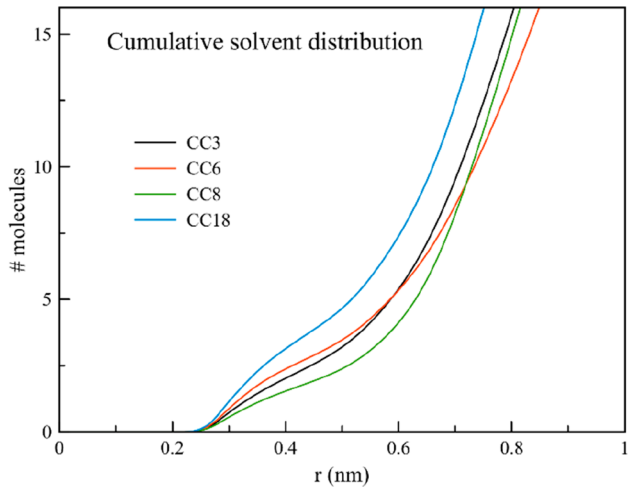

Figure 4. Cumulative distribution of water molecules with respect to the center of mass of the azobenzene core moiety of the cis probes. The maximum water molecules' distance has been set to 0.64 nm.

within a radial distance of 1 nm around the cis conformers with the presence of a steep and nicked curve with a plateau at 0.4 nm from the center of mass, which marks the first solvation shell. The highest amount of water molecules are seen by CC18 due to the well expressed difference in location of this compound with respect to the other ones. Among the others, it is CC8 which bears the least amount of water molecules, which can be linked to its localized and rather slim mass density profile (see Figure 2). The solvent distribution in function of the distance to the probe in Figure 4 is broader and lower for CC3 than for CC6; however, in absence of strong qualitative differences in these plots, the cumulative solvent distributions are virtually identical.

With respect to the embedded probes, the differing amount of water molecules gives rise to different average dipole moments, whose orientation can be investigated by means of the product between the dipole moments of the surrounding water molecules with the vector which connects the solvent dipole with the center of mass of the probe. The differences can be emphasized when the value of the average dipole moment (2.351 ± 0.01 D for all cases) is subtracted. For the cis conformers, the polarization increases along with a generally increasing amount of surrounding water molecules, ranging from 0.41 to 0.60 D. The large radial component of the CC8 conformer (0.60 D) can be explained by the relatively low amount of water molecules in its environment, whose orientation is then also easily affected. Thanks to the molecular geometry and the rather horizontal molecular orientation, the nitrogens of the cis conformer are more vulnerable for through space interactions and π-stacking than in the case of the trans conformers, which are oriented upright and which are consequently only sidewise confronted with water. As a result, while there are virtually no water molecules close to the trans conformers, the N═N bond of the cis faces almost a sphere of molecules, whose orientations are affected by each other.

3. Linear Optical Properties. It is known from literature that the azobenzene molecule does not follow Kasha's rule and the first excited state transition (n → π^*) is forbidden by symmetry in vacuum or in solvents with different polarities, while the first allowed transition is the one to the S_2 which relates to a $\pi \rightarrow \pi^*$ excitation. Although the aim of this work is not to study the photochemistry of conversion of the azobenzene from the trans to the cis isomer, we would like to remark here that this mechanism is still not fully understood, especially when the azobenzene molecule is embedded in biological environments. Yet, already looking at the absorption spectra in the DOPC membrane, it is possible to assess the role of the environment. The one-photon absorption (OPA) spectra of the extracted snapshots from the MD simulations are reported in Figure 5, for both trans and cis isomers.

The first results which can be observed by looking at the absorption spectra are the negligible effect of the tail lengths on the position of the absorption peaks for both isomers. This is not surprising since the frontier orbitals are localized over the aromatic core of the probe. On the one hand, we observe that all the trans isomers present a maximum intensity peak at around 305 nm, arising from the S_2 $\pi \rightarrow \pi^*$ transition, while the cis isomers are peaking at shorter wavelengths at 285 nm with a total blue shift going from trans to cis isomer of 20 nm. On the other hand, the effect of the environment is more visible when the S_1 is analyzed. Now, for both isomers this S_1 is not completely forbidden compared to the case in vacuum, since the twist and bend of the aromatic core along with the conformational motion and the steric hindrance experienced by the probe make the S_1 state weakly allowed. For this transition, it is possible to see a more profound impact of the alkyl tails, as the number of peaks increases with the tail lengths, reflecting a higher conformational change due to the fluctuation of both isomers of the probe in the membrane. Our results are in agreement with dielectric spectroscopy analysis performed on azobenzene derivatives in Langmuir−Blodgett films, which

https://dx.doi.org/10.1021/acs.jpcc.9b11391
J. Phys. Chem. C 2020, 124, 8310−8322

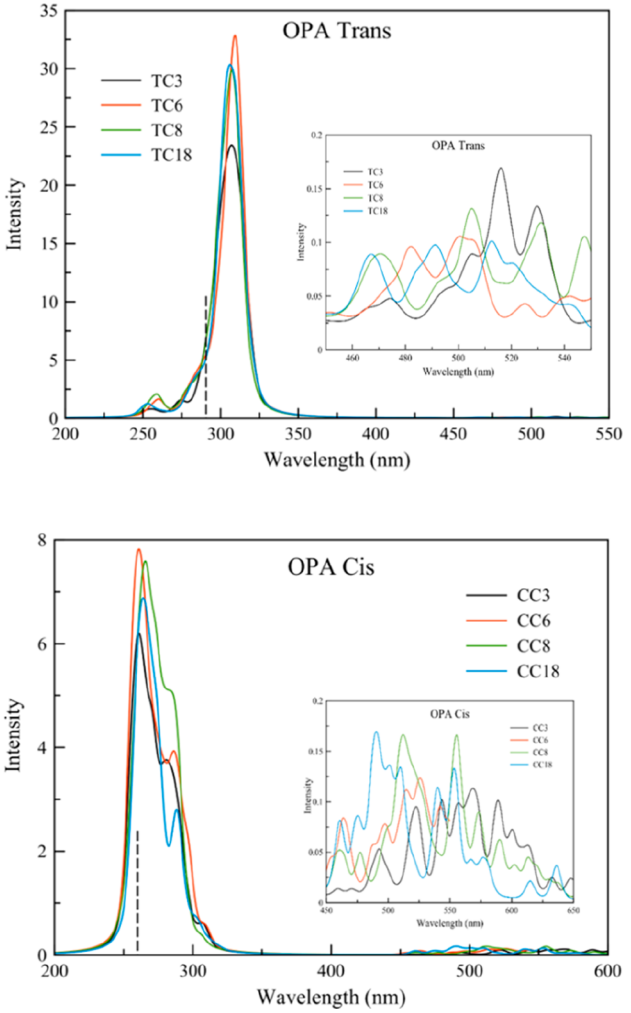

Figure 5. Absorption spectra of the trans and cis isomers of the azobenezene probe embedded in DOPC membrane. All spectra are convolutions over the 50 extracted snapshots for each tail length and isomer. A Lorentzian broadening of 9 nm has been applied, which corresponds to 0.12 eV at 300 nm. The insets are zooms of the S_1 transition, from 450 to 550 nm for the trans isomer and from 450 to 650 nm for the cis isomer. The vertical dashed line refers to S2 of TC3 in vacuum at the ADC(2)/6-31G(d) level of theory.

report that the influence of the local environment upon the switching behavior is much more important than that one of the dipole moments.[89] In addition, as a general remark, we observe that the cis isomers spectra are more complex with respect to the trans ones with S_3 and S_4 transitions strongly allowed and lying at low energy (260 nm). Following the so-called Λ-overlap analysis of Peach et al, which defines the character of the transition (i.e., localized or charge transfer),[90] we compute values of Λ in between 0.5 and 0.7, suggesting a localized character for all transitions of the two isomers with their varying tail lengths. However, the associated orbitals vary from trans to cis. As the S_1 of trans is found to be dark throughout our calculations, it has a profound n → π^* character; the S_2 from the other hand is bright, which is the consequence of a strong $\pi \rightarrow \pi^*$ component. For the cis isomers, the dark S_1 state is characterized by a dominant transition from the highest occupied molecular orbital (H) to the lowest unoccupied one (L); in contradiction to the trans conformer, H has here a strong lone pair character. The S_2 gains oscillator strength thanks to a minor but significant contribution linked to an H-1 →L component, which increases for the compounds with longer tails. A decomposition in terms of molecular orbitals is reported in Table S2, while depictions of the molecular orbitals are given in Figure S7. To provide a benchmark to the presented TDDFT results, additional calculations on the TC3 and CC3 isomers have been performed with the second order Algebraic Diagrammatic Construction scheme [ADC(2)] (see Table S3).[91−93]

4. Nonlinear Optical Properties. The first nonlinear optical (NLO) analysis consists in the study of the two-photon absorption (TPA) ability of the system. TPA is a method of choice when considering the use of such probes in living organisms; since it requires laser beams at a much lower frequency (red or infrared light), causing less damage to the surrounding tissues and cells, it has a higher penetration depth with respect to OPA and enables 3D imaging. The TPA cross section is therefore investigated. From our computations, we found that S_1 is a TPA dark state (see Figure S8), while S_2 is the first TPA active state of interest. The cross section for the S_2 along the various consecutive snapshots is presented in Figure S9 and the full TPA spectra in Figure S10. Different trends can be clearly observed from the strong S_2 TPA state. First of all, the cross section values for the cis isomers are much higher than for the trans isomers, ranging from 150 to 400 GM for all the cis and being 1 order of magnitude lower for all the trans compounds. From the trans isomer, a clear trend is observed for the increasing tails lengths with direct correlation between the length of the alkyl tails and the cross section values in the TC8 > TC6 > TC3 trend while it drops for TC18. A different trend is found for the cis isomers where CC3 and CC6 present lower values of 150 GM, while CC8 and CC18 have a much higher value up to 400 GM. The rationalization of this behavior is two-fold. First, the push effect of the tails over the cis isomers lead it to be an active state, while the pulling effect on the trans isomers is responsible for its inactivity. Second, the environment plays a crucial role in the activity of the isomers, as it affects the transition state dipole moments between excited states, which are of utmost importance in two-photon absorption.[85,94] By reverting to the two state approximation (TSA), we compute the cross section for the CC6 and CC8 probes in order to unravel the large difference observed in values. Since the second excited state is the active state for this analysis, the TSA has been performed on this state only. As reported in Table S4, the cross section values for both CC6 and CC8 are very similar when the TSA is considered. This means that the TPA intensity seen is entirely due to the transition state dipole moments between excited states. Thus, we can conclude that the difference observed rises elsewhere and is not accounted for into the TSA method, which does not fully catch the complexity of the investigated probes.

Since the isomers are found at different locations and orientations in the membrane, the influence of the environment on the excited state properties is clearly visible. As the trans are less affected by the environment due to the deeper position into the membrane bilayer through the pulling effect of the tail, we focus here on the cis isomers in which their relative orientation is a key parameter to consider. In Figure S11, the magnitude of the transition dipole moments between the second and third excited states as well as the second excited state dipole moments obtained through the QM/MM calculations is compared with the ones in which the interaction with the environment is discarded. For the state dipole moments, the results in vacuum

https://dx.doi.org/10.1021/acs.jpcc.9b11391
J. Phys. Chem. C 2020, 124, 8310−8322

are found to be generally less pronounced than the ones in the membranes, clearly pointing at the effect of considering the surrounding for a proper description of the phenomenon, especially when long tails are considered. Our ADC(2) calculations confirm the values obtained in vacuum: the CC3 transition state dipole moment between excited states S_2 and S_3 amounts to 0.90 D, while the state dipole moment of S_2 is found to be 5.35 D. For CAM-B3LYP, these values amount to 1.47 and 5.60 D, respectively (see Figure S12). Thus, when used for TPA analysis, the cis and trans conformers of the azo probes with equal tail lengths present different behaviors in DOPC membrane due to the different push/pull effect; while all the cis isomers can be considered in an active, "on" state, the trans isomers are in a dark, "off" state, making the screening of the membrane effective.

A second parameter which strengthens the push/pull effect is the first hyperpolarizability β. As mentioned in Methods, two different values of β are considered here, namely β_{VEC} and β_{HRS}.

β_{VEC} is inherently connected to the ground state dipole moment (gsdm). Analyzing its values through the QM/MM calculations (see Table S5), we clearly observe the combined effect of the environment and the temperature factor, as it enhances the dipole moment of all trans conformers to a value of 0.50 D, irrespective of the tail length, while in gas phase the trans isomer has a negligible dipole moment. On the other hand, the cis isomers are strongly affected by the presence of the membrane: their gsdm decrease of 50−60% with more fluctuations among the different species due to the different position in the membrane (highhead group density region) compared to the trans isomers (high tail density region).

In contrast to β_{VEC}, β_{HRS} is not affected by the gdsm, and it is obtained considering the vector along the long molecular axis of the probe. Figure 6 reports the β-values for all the probes studied. As already found in our previous study on the DiD probe embedded in different membrane phases,[64] values for β_{HRS} are attenuated by almost 50% compared to β_{VEC}.

A clear trend is present depending on the tail lengths with higher values for the trans isomers up to C6 and a clear inversion for longer tails where the cis isomers become the active state. In detail, the β_{vec} values increase for the trans isomers from 4.7×10^{-30} esu for TC3 up to 6.7×10^{-30} esu for TC6 to suddenly drop to 4.2 and 3.2×10^{-30} esu for TC8 and TC18, respectively. The standard deviations on these values are throughout the study found to be small, less than 12%; data are given in detail in Table S6. At the same time, a constant increase in β_{vec} activity is computed for the cis isomers, going from 3.3×10^{-30} esu for CC3 to similar values of 5.2, 5.5, and 5.0×10^{-30} esu for CC6, CC8, and CC18, respectively. Once more, this can be related to the different push/pull effect of the tails which, in turn, affect the orientation of the probe; for all trans isomers, the aromatic core is strongly tilted and its stiffness is driven by the tail lengths, while for the cis it is perpendicular to the membrane normal. The smaller values obtained for TC3 and CC3 are due to a competition between the push/pull effect of the tails and the hydrophobic/hydrophilic interaction with the membrane; as the tails are short, the latter tend to prevail over the push/pull effect. Yet, the balance is fully shifted toward the former effect as the tail lengths are increased to C6. The smaller value obtained for CC18 is related to the presence of a vast amount of water molecules in the neighborhood, as reported in Figure 4. As a result, there is a direct correlation between the active states and the increase in tail lengths. For shorter tails, up to C6 the trans isomers are the active state, while from C8 onward the situation

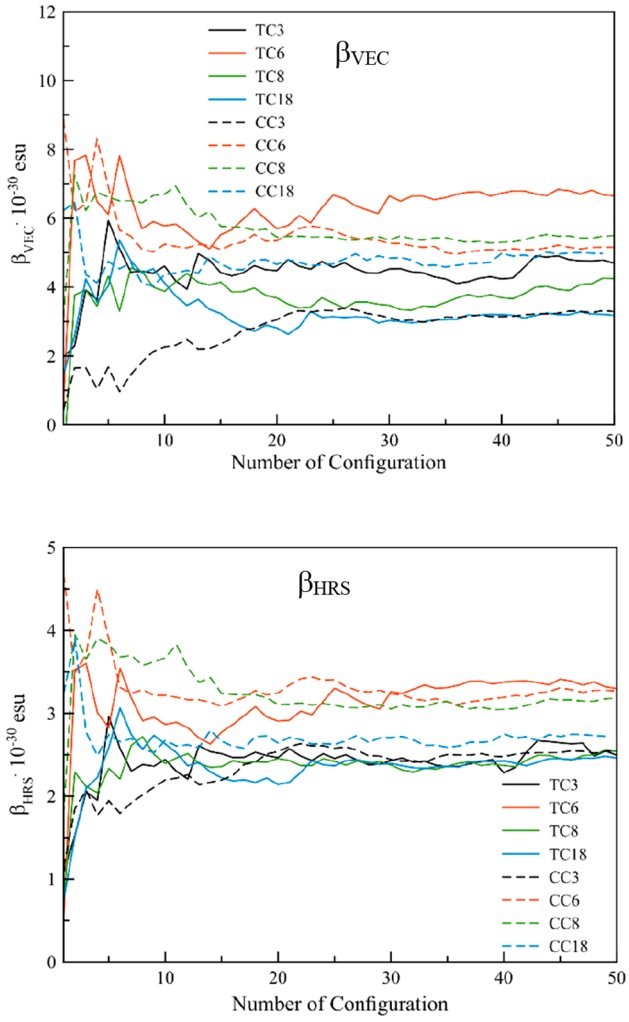

Figure 6. Running average values for β_{VEC} and β_{HRS} for the trans and cis azobenzene probes in DOPC membranes, given in esu units. Only the static component is considered for the analysis. Associated standard deviations are given in Table S6.

is reversed with now the cis isomers being the "on" state. To gain deeper insight, we reverted once more to the TSA (data reported in Table S7). While we observe a quantitative agreement between the two methods for the cis isomers, for the trans conformers the picture is more complex. In fact, values obtained from TSA are up to four times higher than the ones obtained with the full expression, although the trend is qualitatively preserved. This difference is inherent to the nature of the excitation for the trans isomers. In fact, S_2 is now lying at lower energy (4.07 eV) compared to the cis isomers (at around 4.3 eV). In addition, the oscillator strength for the TC is roughly ten times higher than for the CC, which also contributes to the higher values for beta, as well as the possible contribution from higher excited states through their transition state dipole moments.

A similar situation is found for the β_{HRS}, where a general trend is obtained depending on the tail lengths. Now, for short lengths up to C6, it is virtually impossible to distinguish between the trans and cis isomers, which have values of 2.5×10^{-30} esu for C3 and 3.3×10^{-30} esu for C6 (both cis and trans). The lower values for the C3 isomers are once more due to the too short tails which cannot fully counteract electrostatic interaction with the membrane headgroup layer. With longer tails, from C8 onward

https://dx.doi.org/10.1021/acs.jpcc.9b11391
J. Phys. Chem. C 2020, 124, 8310−8322

once more the cis isomers become the active state while the trans are dark, with values of 3.2×10^{-30} esu (2.6×10^{-30} esu) and 2.8×10^{-30} esu (2.5×10^{-30} esu) for CC8 (TC8) and CC18 (TC18), respectively. Once more, this behavior directly relates to the orientation of the aromatic core of the probe and it is more pronounced for the cis isomers, in which longer tails push the molecule in such an orientation that favors the β_{HRS}, while only small wobbling motions are allowed for the trans isomers located deeper in the membrane.

As an introduction to the next paragraph, in which we focus on the second hyperpolarizability and revert to a few-states approximation, we would like to validate the calculation of β in a two-state model using only the components of the ground to excited state transition dipole moment and the state dipole moments of the ground and excited state. The results are given in Table S7. Despite the crude character of the approximation, the results correspond qualitatively to the ones given in Figure 6: the increase toward TC6 and CC6 is well reproduced, along with the decrease toward the obtained values for the isomers with longer tails. The knee seen for the CC8 isomers has become a bit more pronounced and the obtained value is comparable to the one obtained for CC6. For TC8, the obtained β_{HRS} value is a bit lower than the one for TC18. The results seem therefore to emphasize the usefulness of a limited model, like already remarked by Meyers et al.[95] We remark that the differences between the values obtained by the full expression and the two state model are by definition linked to the transition state dipole moments between excited states and the absence of higher excited states.

The next parameter considered is the third order polarizability γ. Although much smaller in absolute values compared to the other two parameters, this analysis is needed to enable the forthcoming discussion of the second order susceptibility. In response theory, the second residue of γ gives access to transition dipole moments between excited states, and following its derivation the imaginary part of the orientationally averaged third order polarizability is proportional to the two-photon absorption cross section.[85,96] As the first active excited state is S_2, we considered the few states model for γ discussed above and used this particular excited state as the intermediate state e mentioned in the dipole, two-photon, and negative terms (results are reported in Figure S13). Interestingly, we observe that all trans isomers have higher values of γ (with average value going from 2.1 to 2.9×10^{-36} esu) compared to the cis ones ($1.2-2.2 \times 10^{-36}$ esu), irrespective of the tail lengths, making the trans isomer the active state for this analysis.

Finally using eq 2, we can compute the second susceptibility $\chi^{(2)}$, which gives rise to the signal obtained through second harmonic generation measurements.[77] With respect to the difference in orientation of the trans and cis isomers and referring to available surface pressure-molecular area isotherms measurements, strong differences in susceptibilities can be expected.[97]

From the data depicted in Figure 7, the first striking result is that susceptibility values for the cis isomers are higher than the trans of at least 1 order of magnitude, making the cis isomers the active state in EFISHG. Once more, C3 isomers (both trans and cis) show a peculiar behavior for the reasons discussed above and starting from C6 we observe the presence of an inverse correlation for the trans isomer, where the susceptibility constantly decreases with an increasing tail length and with values in the $7-20 \times 10^{-36}$ esu range. On the other hand, the increase in tail lengths is the driving force for the cis isomers. In

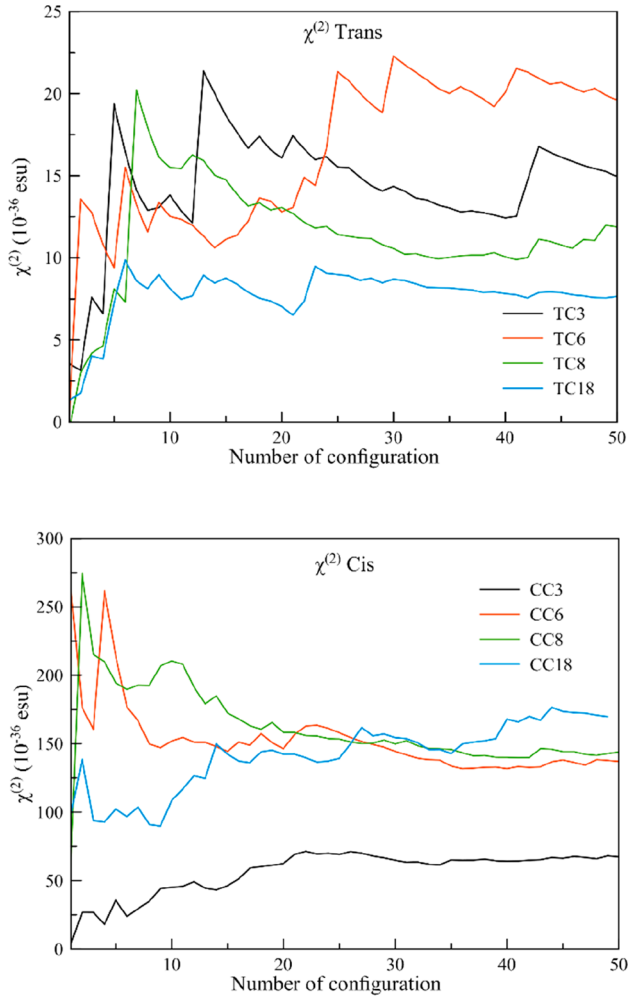

Figure 7. Running average of the second susceptibility analysis in esu units for all trans and cis isomers. All values are obtained at 323 K. Associated standard deviations are given in Table S6.

fact, the susceptibility strongly increases, going from values of 62×10^{-36} esu for CC3 up to 160×10^{-36} esu for CC18 clearly showing the importance of the push and pull effects of the tails for the cis and trans isomers, respectively.

CONCLUSIONS

The conformationally versatile azobenzene molecule has been used as a lipid bilayer probe for phase recognition. The influence of alkyl tails on the location, orientation, and (non)linear optical properties of the probe has been investigated by considering trans and cis isomers with symmetric tails of length 3, 6, 8, and 18 carbon atoms. Strikingly, for cis azobenzene the series of increasing tails were found to push the core of the chromophore toward the polar membrane surface, while for the trans isomer the tails were rather found to exhibit a pulling effect toward the membrane center. All the trans isomers are located deep in the membrane and have an orientation slightly tilted with respect to the membrane normal, while the cis ones can be found closer to the polar headgroup region. The azo-core of the latter conformers are found with their main axis more parallel to the membrane surface, which also affects the influence of the isomers on the orientation of the surrounding water molecules. As a consequence, the photoselection of the cis isomer with the

https://dx.doi.org/10.1021/acs.jpcc.9b11391
J. Phys. Chem. C 2020, 124, 8310−8322

longest alkyl chains by means of a beam with field vector perpendicular to the membrane surface is rather minimal.

The correlation between the tails and their pushing effect for cis azobenzene is strikingly seen in the nonlinear optical spectroscopies. The S_2 is the active state in two-photon absorption and its cross section increases along with the tail length; it is connected to the transition state dipole moments between the excited states which change along. For the deep lying trans isomer, the distance to the polar groups increases with increasing tail length, and the TPA cross section is found to be unaffected by the environment. On the other hand, for the cis isomers the pushing effect of the tails leads to be the active state for the TPA analysis with cross section values 10 times higher with respect to the trans. Throughout the analysis of the static component of the first and second hyperpolarizabilities, a neat distinction between the tail lengths is observed; for shorter tails (up to C6) the trans isomer is the active state, while a further increase of the tail lengths lead to a switch in the behavior with now the cis isomer being the active state. Finally, the investigation of the simulated second susceptibility $\chi^{(2)}$, observed in second harmonic generation measurements, shows that the cis isomers have values 10 times higher than the trans ones, irrespective of the tail lengths, making this isomer the active state.

As the push/pull effect is strongly coupled to the NLO properties, it should be considered in forthcoming developments of photosensitive probes for membrane recognition. To use them to discriminate between healthy and unhealthy membranes, the influence of the tail lengths of the embedded probes on the excited state lifetimes has to be investigated by time-resolved fluorescence spectroscopy. The current work presents the state of the art for the simulation, analysis, and interpretation of (non) linear optical spectroscopy studies on chromophores and conformationally versatile molecular probes embedded in lipid bilayers and lays the foundations for further investigations.

■ ASSOCIATED CONTENT

Supporting Information

The Supporting Information is available free of charge at https://pubs.acs.org/doi/10.1021/acs.jpcc.9b11391.

Nonstandard force-field parameters for azobenzene; full expression for the second hyperpolarizability in the essential state model; dipolar term for the first hyperpolarizability and the TPA cross section; CNNC dihedral angle analysis; density profile of the whole trans isomer and the two methyl groups at the end of the alkyl tails; HOMO of CC18 in a DOPC lipid bilayer; position of the center of mass of the two phenyl rings (dubbed Ph-1 and Ph-2) of the CC3, CC6, and CC8 isomers; representative structures for the eight azo isomers considered in this study; distribution of the angle between the normal to the phenyl rings of the probe and the normal to the membrane surface for both trans and cis isomers; absorption properties for the first two excited states of the probes in DOPC; frontier orbitals for TC3 and CC3; ADC(2) excited state energies; TPA cross section in GM units of the S_1 excited state for both trans and cis isomers; TPA cross section for TPA in GM units of the S_2 excited state for both trans and cis isomers; two-photon absorption spectra for all the considered trans and cis isomers; transition state dipole moments between the second and third excited states and second excited state dipole moments for the cis azobenzene isomers in function of their tail lengths; basis set dependence of the TPA cross section for the S_1 and S_2 excited states; values of the ground state dipole moments of the different species and conformers; average values and the standard deviations of the computed NLO quantities; values for β_{HRS} calculated by means of a two-state model; results for the dipolar approximation of the TPA cross section for CC6 and CC8; orientationally averaged second order hyperpolarizability γ (PDF)

■ AUTHOR INFORMATION

Corresponding Authors

Stefan Knippenberg − *Theoretical Physics, Hasselt University, 3590 Diepenbeek, Belgium; Department of Theoretical Chemistry and Biology, School of Engineering Sciences in Chemistry, Biotechnology and Health, KTH Royal Institute of Technology, SE-10691 Stockholm, Sweden; Research Group PLASMANT, Department of Chemistry, University of Antwerp, B-2610 Antwerp, Belgium; RCPTM, Department of Physical Chemistry, Faculty of Sciences, Palacký University, Olomouc, Czech Republic;* orcid.org/0000-0002-4527-2566; Email: stefan.knippenberg@upol.cz

Silvio Osella − *Biological Systems Simulation Lab, Centre of New Technologies, University of Warsaw, 02-097 Warsaw, Poland;* orcid.org/0000-0001-8541-1914; Email: s.osella@cent.uw.edu.pl

Complete contact information is available at: https://pubs.acs.org/10.1021/acs.jpcc.9b11391

Notes

The authors declare no competing financial interest.

■ ACKNOWLEDGMENTS

S.O. acknowledges the National Science Centre, Poland, (Grant UMO-2018/31/D/ST4/01475) for the funding. S.K. is grateful to the Czech Science Foundation through Grant 17-21122S. For the computational time, the authors thank the Swedish National Infrastructure for Computing (SNIC) for the medium allocations in 2017 (1-16, 1-102) and 2018 (3-397, 3-156, 3-396, 3-23), the Interdisciplinary Center for Mathematical and Computational Modelling (ICM, University of Warsaw) under the GA53-8, GA73-16, and GA76-5 computational grants, and the Flemish Supercomputer Centre (VSC) along with the Herculesstichting (Flanders, Belgium) for the access to the Breniac and Genius clusters.

■ REFERENCES

(1) Willner, I.; Rubin, S. Control of the Structure and Functions of Biomaterials by Light. *Angew. Chem., Int. Ed. Engl.* **1996**, *35*, 367−385.

(2) Willner, I. Photoswitchable Biomaterials: En Route to Optobioelectronic Systems. *Acc. Chem. Res.* **1997**, *30*, 347−356.

(3) Dyck, R. H.; McClure, D. S. Ultraviolet Spectra of Stilbene, p-Monohalogen Stilbenes, and Azobenzene and the trans to cis Photoisomerization Process. *J. Chem. Phys.* **1962**, *36*, 2326.

(4) Jaffe, H.; Yeh, S.; Gardner, R. The Electronic Spectra of Azobenzene Derivatives and Their Conjugate Acids. *J. Mol. Spectrosc.* **1958**, *2*, 120−136.

(5) Turro, N. J.; Ramamurthy, V.; Scaiano, J. C. *Modern Molecular Photochemistry of Organic Molecules*; University Science Books: Mill Valley, CA, 2010.

(6) Yang, C.; Slavov, C.; Wegner, H. A.; Wachtveitl, J.; Dreuw, A. Computational Design of a molecular Triple Photoswitch for Wavelength-Selective Control. *Chem. Sci.* **2018**, *9*, 8665−8672.
(7) Slavov, C.; Yang, C.; Schweighauser, L.; Wegner, H. A.; Dreuw, A.; Wachtveitl, J. Ultrafast Excited-State Deactivation Dynamics of Cyclotrisazobenzene-A Novel Type of UV-B Absorber. *ChemPhysChem* **2017**, *18*, 2137−2141.
(8) Slavov, C.; Yang, C.; Schweighauser, L.; Boumrifak, C.; Dreuw, A.; Wegner, H. A.; Wachtveitl, J. Connectivity Matters - Ultrafast Isomerization Dynamics of Bisazobenzene Photoswitches. *Phys. Chem. Chem. Phys.* **2016**, *18*, 14795−14804.
(9) Slavov, C.; Yang, C.; Heindl, A. H.; Stauch, T.; Wegner, H. A.; Dreuw, A.; Wachtveitl, J. Twist and Return-Induced Ring Strain Triggers Quick Relaxation of a (Z)-Stabilized Cyclobisazobenzene. *J. Phys. Chem. Lett.* **2018**, *9*, 4776−4781.
(10) Browne, W. R.; Feringa, B. L. Making Molecular Machines Work. *Nat. Nanotechnol.* **2006**, *1*, 25−35.
(11) Wachtveitl, J.; Sporlein, S.; Satzger, H.; Fonrobert, B.; Renner, C.; Behrendt, R.; Oesterhelt, D.; Moroder, L.; Zinth, W. Ultrafast Conformational Dynamics in Cyclic Azobenzene Peptides of Increased Flexibility. *Biophys. J.* **2004**, *86*, 2350−2362.
(12) Hugel, T.; Holland, N. B.; Cattani, A.; Moroder, L.; Seitz, M.; Gaub, H. E. Single-Molecule Optomechanical Cycle. *Science* **2002**, *296*, 1103−1106.
(13) Kumar, G.; Neckers, D. Photochemistry of Azobenzene-Containing Polymers. *Chem. Rev.* **1989**, *89*, 1915−1925.
(14) Liu, Z.; Hashimoto, K.; Fujishima, A. Photoelectrochemical Information-Storage Using an Azobenzene Derivative. *Nature* **1990**, *347*, 658−660.
(15) Ikeda, T.; Tsutsumi, O. Optical Switching and Image Storage by Means of Azobenzene Liquid-Crystal Films. *Science* **1995**, *268*, 1873−1875.
(16) Natansohn, A.; Rochon, P. Photoinduced Motions in Azo-Containing Polymers. *Chem. Rev.* **2002**, *102*, 4139−4175.
(17) Yu, Y. L.; Nakano, M.; Ikeda, T. Directed Bending of a Polymer Film by Light - Miniaturizing a Simple Photomechanical System Could Expand its Range of Applications. *Nature* **2003**, *425*, 145−145.
(18) Banerjee, I. A.; Yu, L. T.; Matsui, H. Application of Host-Guest Chemistry in Nanotube-Based Device Fabrication: Photochemically Controlled Immobilization of Azobenzene Nanotubes on Patterned Alpha-CD Monolayer/Au Substrates via Molecular Recognition. *J. Am. Chem. Soc.* **2003**, *125*, 9542−9543.
(19) Feringa, B. L. *Molecular Switches*; Wiley-VCH: Weinheim, 2001.
(20) Shinkai, S.; Honda, Y.; Ueda, K.; Manabe, O. Photoresponsive Crown Ethers 0.12. Photocontrol of Metal-Ion Complexation with Thiacrown Ethers. *Bull. Chem. Soc. Jpn.* **1984**, *57*, 2144−2149.
(21) Rojanathanes, R.; Pipoosananakaton, B.; Tuntulani, T.; Bhanthumnavin, W.; Orton, J. B.; Cole, S. J.; Hursthouse, M. B.; Grossel, M. C.; Sukwattanasinitt, M. Comparative Study of Azobenzene and Stilbene Bridged Crown Ether p-tert-butylcalix[4]arene. *Tetrahedron* **2005**, *61*, 1317−1324.
(22) McSkimming, G.; Tucker, J. H. R.; Bouas-Laurent, H.; Desvergne, J. P.; Coles, S. J.; Hursthouse, M. B.; Light, M. E. Photoinduced Formation of a Cryptand from a Coronand: An Unexpected Switch in Cation Binding Affinity. *Chem. - Eur. J.* **2002**, *8*, 3331−3342.
(23) Chang, C. W.; Lu, Y. C.; Wang, T. T.; Diau, E. W. G. Photoisomerization Dynamics of Azobenzene in Solution with S-1 Excitation: A Femtosecond Fluorescence Anisotropy Study. *J. Am. Chem. Soc.* **2004**, *126*, 10109−10118.
(24) Cusati, T.; Granucci, G.; Persico, M. Photodynamics and Time-Resolved Fluorescence of Azobenzene in Solution: A Mixed Quantum-Classical Simulation. *J. Am. Chem. Soc.* **2011**, *133*, 5109−5123.
(25) Osella, S.; Knippenberg, S. Triggering On/Off States of Photoswitchable Probes in Biological Environments. *J. Am. Chem. Soc.* **2017**, *139*, 4418−4428.
(26) Goossens, P.; Rodriguez-Vita, J.; Etzerodt, A.; Masse, M.; Rastoin, O.; Gouirand, V.; Ulas, T.; Papantonopoulou, O.; Van Eck, M.; Auphan-Anezin, N.; et al. Membrane Cholesterol Efflux Drives Tumor-Associated Macrophage Reprogramming and Tumor Progression. *Cell Metab.* **2019**, *29*, 1376−1389.
(27) Erazo-Oliveras, A.; Fuentes, N. R.; Wright, R. C.; Chapkin, R. S. Functional Link between Plasma Membrane Spatiotemporal Dynamics, Cancer Biology, and Dietary Membrane-Altering Agents. *Cancer Metastasis Rev.* **2018**, *37*, 519−544.
(28) Filipova, L.; Kohagen, M.; Stacko, P.; Muchova, E.; Slavicek, P.; Klan, P. Photoswitching of Azobenzene-Based Reverse Micelles above and at Subzero Temperatures as Studied by NMR and Molecular Dynamics Simulations. *Langmuir* **2017**, *33*, 2306−2317.
(29) Unksov, I. N.; Kasyanenko, N. A. Conformational Changes in the Dna Molecule in Solution Caused by the Binding of a Light-Sensitive Cationic Surfactant. *J. Struct. Chem.* **2017**, *58*, 413−419.
(30) Kasyanenko, N.; Lysyakova, L.; Ramazanov, R.; Nesterenko, A.; Yaroshevich, I.; Titov, E.; Alexeev, G.; Lezov, A.; Unksov, I. Conformational and Phase Transitions in DNA-Photosensitive Surfactant Solutions: Experiment and Modeling. *Biopolymers* **2015**, *103*, 109−122.
(31) Rastaedter, D.; Biswas, M.; Burghardt, I. Molecular Dynamics Study of the Controlled Destabilization of an RNA Hairpin Structure by a Covalently Attached Azobenzene Switch. *J. Phys. Chem. B* **2014**, *118*, 8478−8488.
(32) McCullagh, M.; Franco, I.; Ratner, M. A.; Schatz, G. C. Defects in DNA: Lessons from Molecular Motor Design. *J. Phys. Chem. Lett.* **2012**, *3*, 689−693.
(33) Wu, L.; Koumoto, K.; Sugimoto, N. Reversible Stability Switching of a Hairpin DNA via a Photo-Responsive Linker Unit. *Chem. Commun.* **2009**, 1915−1917.
(34) Boeckmann, M.; Peter, C.; Delle Site, L.; Doltsinis, N. L.; Kremer, K.; Marx, D. Atomistic Force Field for Azobenzene Compounds Adapted for QM/MM Simulations with Applications to Liquids and Liquid Crystals. *J. Chem. Theory Comput.* **2007**, *3*, 1789−1802.
(35) Xia, S.-H.; Cui, G.; Fang, W.-H.; Thiel, W. How Photoisomerization Drives Peptide Folding and Unfolding: Insights from QM/MM and MM Dynamics Simulations. *Angew. Chem., Int. Ed.* **2016**, *55*, 2067−2072.
(36) Nuti, F.; Gellini, C.; Larregola, M.; Squillantini, L.; Chelli, R.; Salvi, P. R.; Lequin, O.; Pietraperzia, G.; Papini, A. M. A Photochromic Azobenzene Peptidomimetic of a beta-Turn Mode Peptide Structure as a Conformational Switch. *Front. Chem.* **2019**, *7*, 180.
(37) Opie, C. R.; Kumagai, N.; Shibasaki, M. Reversible Stereoselective Folding/Unfolding Fueled by the Interplay of Photoisomerism and Hydrogen Bonding. *Angew. Chem., Int. Ed.* **2017**, *56*, 3349−3353.
(38) Lorenz, L.; Kusebauch, U.; Moroder, L.; Wachtveitl, J. Temperature- and Photocontrolled Unfolding/Folding of a Triple-Helical Azobenzene-Stapled Collagen Peptide Monitored by Infrared Spectroscopy. *ChemPhysChem* **2016**, *17*, 1314−1320.
(39) Mueller, A.; Kobarg, H.; Chandrasekaran, V.; Gronow, J.; Soennichsen, F. D.; Lindhorst, T. K. Synthesis of Bifunctional Azobenzene Glycoconjugates for Cysteine-Based Photosensitive Cross-Linking with Bioactive Peptides. *Chem. - Eur. J.* **2015**, *21*, 13723−13731.
(40) Chandramouli, B.; Di Maio, D.; Mancini, G.; Brancato, G. Introducing an Artificial Photo-Switch into a Biological Pore: A Model Study of an Engineered alpha-Hemolysin. *Biochim. Biophys. Acta, Biomembr.* **2016**, *1858*, 689−697.
(41) Merino, E.; Ribagorda, M. Control over Molecular Motion Using the cis-trans Photoisomerization of the Azo Group. *Beilstein J. Org. Chem.* **2012**, *8*, 1071−1090.
(42) Banghart, M. R.; Volgraf, M.; Trauner, D. Engineering Light-Gated Ion Channels. *Biochemistry* **2006**, *45*, 15129−15141.
(43) Jog, P. V.; Gin, M. S. A Light-Gated Synthetic Ion Channel. *Org. Lett.* **2008**, *10*, 3693−3696.
(44) Yoon, Z. S.; Kwon, J. H.; Yoon, M.-C.; Koh, M. K.; Noh, S. B.; Sessler, J. L.; Lee, J. T.; Seidel, D.; Aguilar, A.; Shimizu, S.; et al. Nonlinear Optical Properties and Excited-State Dynamics of Highly

https://dx.doi.org/10.1021/acs.jpcc.9b11391
J. Phys. Chem. C 2020, 124, 8310−8322

Symmetric Expanded Porphyrins. *J. Am. Chem. Soc.* **2006**, *128*, 14128−14134.
(45) Woller, T.; Geerlings, P.; De Proft, F.; Champagne, B.; Alonso, M. Aromaticity as a Guiding Concept for Spectroscopic Features and Nonlinear Optical Properties of Porphyrinoids. *Molecules* **2018**, *23*, 1333.
(46) Yoon, Z. S.; Cho, D.-G.; Kim, K. S.; Sessler, J. L.; Kim, D. Nonlinear Optical Properties as a Guide to Aromaticity in Congeneric Pentapyrrolic Expanded Porphyrins: Pentaphyrin, Sapphyrin, Isosmaragdyrin, and Orangarin. *J. Am. Chem. Soc.* **2008**, *130*, 6930−6931.
(47) Pawlicki, M.; Collins, H. A.; Denning, R. G.; Anderson, H. L. Two-Photon Absorption and the Design of Two-Photon Dyes. *Angew. Chem., Int. Ed.* **2009**, *48*, 3244−3266.
(48) Naoda, K.; Mori, H.; Aratani, N.; Lee, B. S.; Kim, D.; Osuka, A. Hexaphyrin Fused to Two Anthracenes. *Angew. Chem., Int. Ed.* **2012**, *51*, 9856−9859.
(49) Rath, H.; Prabhuraja, V.; Chandrashekar, T. K.; Nag, A.; Goswami, D.; Joshi, B. S. Aromatic Core Modified Decaphyrins with the Largest Two-Photon Absorption Cross-Sections: Syntheses and Characterization. *Org. Lett.* **2006**, *8*, 2325−2328.
(50) Higashino, T.; Nakatsuji, H.; Fukuda, R.; Okamoto, H.; Imai, H.; Matsuda, T.; Tochio, H.; Shirakawa, M.; Tkachenko, N. V.; Hashida, M.; et al. Hexaphyrin as a Potential Theranostic Dye for Photothermal Therapy and 19F Magnetic Resonance Imaging. *ChemBioChem* **2017**, *18*, 951−959.
(51) Pielak, K.; Bondu, F.; Sanguinet, L.; Rodriguez, V.; Champagne, B.; Castet, F. Second-Order Nonlinear Optical Properties of Multiaddressable Indolinooxazolidine Derivatives: Joint Computational and Hyper-Rayleigh Scattering Investigations. *J. Phys. Chem. C* **2017**, *121*, 1851−1860.
(52) Bondu, F.; Hadji, R.; Szaloki, G.; Aleveque, O.; Sanguinet, L.; Pozzo, J.-L.; Cavagnat, D.; Buffeteau, T.; Rodriguez, V. Huge Electro-/Photo-/Acidoinduced Second-Order Nonlinear Contrasts from Multiaddressable Indolinooxazolodine. *J. Phys. Chem. B* **2015**, *119*, 6758−6765.
(53) Song, X. D.; Perlstein, J.; Whitten, D. G. Supramolecular Aggregates of Azobenzene Phospholipids and Related Compounds in Bilayer Assemblies and other Microheterogeneous Media: Structure, Properties, and Photoreactivity. *J. Am. Chem. Soc.* **1997**, *119*, 9144−9159.
(54) Pernpeintner, C.; Frank, J. A.; Urban, P.; Roeske, C. R.; Pritzl, S. D.; Trauner, D.; Lohmueller, T. Light-Controlled Membrane Mechanics and Shape Transitions of Photoswitchable Lipid Vesicles. *Langmuir* **2017**, *33*, 4083−4089.
(55) Osella, S.; Murugan, N. A.; Jena, N. K.; Knippenberg, S. Investigation into Biological Environments through (Non)linear Optics: A Multiscale Study of Laurdan Derivatives. *J. Chem. Theory Comput.* **2016**, *12*, 6169−6181.
(56) Cornelis, D.; Franz, E.; Asselberghs, I.; Clays, K.; Verbiest, T.; Koeckelberghs, G. Interchromophoric Interactions in Chiral X-type pi-Conjugated Oligomers: A Linear and Nonlinear Optical Study. *J. Am. Chem. Soc.* **2011**, *133*, 1317−1327.
(57) Van Der Spoel, D.; Lindahl, E.; Hess, B.; Groenhof, G.; Mark, A. E.; Berendsen, H. J. C. GROMACS: Fast, Flexible, and Free. *J. Comput. Chem.* **2005**, *26*, 1701−1718.
(58) Hess, B.; Kutzner, C.; van der Spoel, D.; Lindahl, E. GROMACS 4: Algorithms for Highly Efficient, Load-Balanced, and Scalable Molecular Simulation. *J. Chem. Theory Comput.* **2008**, *4*, 435−447.
(59) Pandit, S. A.; Vasudevan, S.; Chiu, S. W.; Jay Mashl, R.; Jakobsson, E.; Scott, H. L. Sphingomyelin-Cholesterol Domains in Phospholipid Membranes: Atomistic Simulation. *Biophys. J.* **2004**, *87*, 1092−1100.
(60) Pandit, S. A.; Chiu, S.-W.; Jakobsson, E.; Grama, A.; Scott, H. L. Cholesterol Packing Around Lipids with Saturated and Unsaturated Chains: A Simulation Study. *Langmuir* **2008**, *24*, 6858−6865.
(61) Chiu, S. W.; Vasudevan, S.; Jakobsson, E.; Mashl, R. J.; Scott, H. L. Structure of Sphingomyelin Bilayers: a Simulation Study. *Biophys. J.* **2003**, *85*, 3624−3635.
(62) Pandit, S. A.; Chiu, S.-W.; Jakobsson, E.; Grama, A.; Scott, H. L. Cholesterol Surrogates: A Comparison of Cholesterol and 16:0 Ceramide in POPC Bilayers. *Biophys. J.* **2007**, *92*, 920−927.
(63) Paloncýová, M.; Aniander, G.; Larsson, E.; Knippenberg, S. Cyanine Dyes with Tail Length Asymmetry Enhance Photoselection: A Multiscale Study on DiD Probes in a Liquid Disordered Membrane. *Spectrochim. Acta, Part A* **2020**, *224*, 117329.
(64) Osella, S.; Di Meo, F.; Murugan, N. A.; Fabre, G.; Ameloot, M.; Trouillas, P.; Knippenberg, S. Combining (Non)linear Optical and Fluorescence Analysis of DiD to Enhance Lipid Phase Recognition. *J. Chem. Theory Comput.* **2018**, *14*, 5350−5359.
(65) Knippenberg, S.; Fabre, G.; Osella, S.; Di Meo, F.; Paloncyova, M.; Ameloot, M.; Trouillas, P. Atomistic Picture of Fluorescent Probes with Hydrocarbon Tails in Lipid Bilayer Membranes: An Investigation of Selective Affinities and Fluorescent Anisotropies in Different Environmental Phases. *Langmuir* **2018**, *34*, 9072−9084.
(66) Nose, S. A Unified Formulation of the Constant Temperature Molecular-Dynamics Methods. *J. Chem. Phys.* **1984**, *81*, 511−519.
(67) Hoover, W. G. Canonical dynamics: Equilibrium phase-space distributions. *Phys. Rev. A: At., Mol., Opt. Phys.* **1985**, *31*, 1695−1697.
(68) Parrinello, M.; Rahman, A. Polymorphic Transitions in Single-Crystals - a New Molecular-Dynamics Method. *J. Appl. Phys.* **1981**, *52*, 7182−7190.
(69) Darden, T.; York, D.; Pedersen, L. Particle Mesh Ewald: An N·log(N) Method for Ewald Sums in Large Systems. *J. Chem. Phys.* **1993**, *98*, 10089−10092.
(70) Leonenko, Z. V.; Finot, E.; Ma, H.; Dahms, T. E. S.; Cramb, D. T. Investigation of Temperature-Induced Phase Transitions in DOPC and DPPC Phospholipid Bilayers Using Temperature-Controlled Scanning Force Microscopy. *Biophys. J.* **2004**, *86*, 3783−3793.
(71) Wang, J. M.; Cieplak, P.; Kollman, P. A. How Well does a Restrained Electrostatic Potential (RESP) Model Perform in Calculating Conformational Energies of Organic and Biological Molecules? *J. Comput. Chem.* **2000**, *21*, 1049−1074.
(72) Frisch, M. J.; Trucks, G. W.; Schlegel, H. B.; Scuseria, G. E.; Robb, M. A.; Cheeseman, J. R.; Scalmani, G.; Barone, V.; Mennucci, B.; Petersson, G. A.; et al. *Gaussian 09*, Revision D.1; Gaussian, Inc.: Wallingford, CT, 2009.
(73) Yanai, T.; Tew, D. P.; Handy, N. C. A New Hybrid Exchange-Correlation Functional Using the Coulomb-Attenuating Method (CAM-B3LYP). *Chem. Phys. Lett.* **2004**, *393*, 51−57.
(74) Dunning, T. Gaussian-Basis Sets for Use in Correlated Molecular Calculations 0.1. the Atoms Boron Through Neon and Hydrogen. *J. Chem. Phys.* **1989**, *90*, 1007−1023.
(75) Aidas, K.; Angeli, C.; Bak, K. L.; Bakken, V.; Bast, R.; Boman, L.; Christiansen, O.; Cimiraglia, R.; Coriani, S.; Dahle, P.; et al. The Dalton Quantum Chemistry Program System. *Wiley Interdiscip. Rev.-Comput. Mol. Sci.* **2014**, *4*, 269−284.
(76) Osella, S.; Knippenberg, S. Laurdan as Molecular Rotor in Biological Environments. *ACS Appl. Bio Mater.* **2019**, *2*, 5769−5778.
(77) Sundholm, D.; Rizzo, A.; Jorgensen, P. Multiconfiguration Self-Consistent-Field Quadratic Response Calculations. *J. Chem. Phys.* **1994**, *101*, 4931−4935.
(78) Ostroverkhova, O.; Stickrath, A.; Singer, K. D. Electric Field-Induced Second Harmonic Generation Studies of Chromophore Orientational Dynamics in Photorefractive Polymers. *J. Appl. Phys.* **2002**, *91*, 9481.
(79) Asselberghs, I.; Pérez-Moreno, J.; Clays, K. In *Non-Linear Optical Properties of Matter: From Molecules to Condensed Phases*; Papadopoulos, G. M.; Sadlej, A. J.; Leszczynski, J. Eds.; Springer Netherlands: Dordrecht, 2006; pp 419−459.
(80) Dworczak, R.; Kieslinger, D. Electric Field Induced Second Harmonic Generation (EFISH) Experiments in the Swivel Cell: New Aspects of an Established Method. *Phys. Chem. Chem. Phys.* **2000**, *2*, 5057−5064.
(81) Hu, Z.; Autschbach, J.; Jensen, L. Simulation of Resonance Hyper-Rayleigh Scattering of Molecules and Metal Clusters Using a Time-Dependent Density Functional Theory Approach. *J. Chem. Phys.* **2014**, *141*, 124305.

https://dx.doi.org/10.1021/acs.jpcc.9b11391
J. Phys. Chem. C 2020, 124, 8310−8322

(82) Orr, B. J.; Ward, J. F. Perturbation Theory of the Non-Linear Optical Polarization of an Isolated System. *Mol. Phys.* **1971**, *20*, 513−526.
(83) Dirk, C.; Cheng, L.; Kuzyk, M. A Simplified 3-Level Model Describing the Molecular 3rd-Order Nonlinear Optical Susceptibility. *Int. J. Quantum Chem.* **1992**, *43*, 27−36.
(84) Garito, A. F.; Teng, C. C. Nonlinear Optical Processes In Organic Media: Large Non-Resonant Third Order Electronic Responses In High Performance Liquid Crystal Polymer Structures. *Proc. SPIE 0613, Nonlinear Optics and Applications*; Yeh, P., Ed.; Society of Photo-Optical Instrumentation Engineers: Los Angeles, CA, 1986.
(85) Knippenberg, S.; Gieseking, R. L.; Rehn, D. R.; Mukhopadhyay, S.; Dreuw, A.; Bredas, J.-L. Benchmarking Post-Hartree-Fock Methods to Describe the Nonlinear Optical Properties of Polymethines: An Investigation of the Accuracy of Algebraic Diagrammatic Construction (ADC) Approaches. *J. Chem. Theory Comput.* **2016**, *12*, 5465−5476.
(86) Marrink, S.; Berendsen, H. Simulation of Water Transport Through a Lipid-Membrane. *J. Phys. Chem.* **1994**, *98*, 4155−4168.
(87) Wang, D.; Wang, X. Amphiphilic Azo Polymers: Molecular Engineering, Self-Assembly and Photoresponsive Properties. *Prog. Polym. Sci.* **2013**, *38*, 271−301.
(88) Lakowicz, J. R. *Principles of Fluorescence Spectroscopy*, 3rd ed.; Springer, 2007.
(89) Buchsteiner, A.; Brehmer, L. Investigation of Order and Optical Switching in Ultrathin Films of Azo-Containing Materials Using Dielectric Spectroscopy. *IEEE Trans. Dielectr. Electr. Insul.* **2001**, *8*, 516−521.
(90) Peach, M. J. G.; Benfield, P.; Helgaker, T.; Tozer, D. J. Excitation Energies in Density Functional Theory: An Evaluation and a Diagnostic Test. *J. Chem. Phys.* **2008**, *128*, 044118.
(91) Schirmer, J. Beyond the Random-Phase Approximation: A new Approximation Scheme for the Polarization Propagator. *Phys. Rev. A: At., Mol., Opt. Phys.* **1982**, *26*, 2395−2416.
(92) Wormit, M.; Rehn, D. R.; Harbach, P. H. P.; Wenzel, J.; Krauter, C. M.; Epifanovsky, E.; Dreuw, A. Investigating Excited Electronic States Using the Algebraic Diagrammatic Construction (ADC) Approach of the Polarisation Propagator. *Mol. Phys.* **2014**, *112*, 774.
(93) Dreuw, A.; Wormit, M. The Algebraic Diagrammatic Construction Scheme for the Polarization Propagator for the Calculation of Excited States. *Wiley Interdiscip. Rev.-Comput. Mol. Sci.* **2015**, *5*, 82−95.
(94) Bishop, D. M. Explicit Nondivergent Formulas for Atomic and Molecular Dynamic Hyperpolarizabilities. *J. Chem. Phys.* **1994**, *100*, 6535.
(95) Meyers, F.; Marder, S.; Pierce, B.; Bredas, J.-L. Electric-Field Modulated Nonlinear-Optical Properties of Donor-Acceptor Polyenes - Sum-Over-States Investigation of the Relationship Between Molecular Polarizabilities (alpha, Beta, and Gamma) and Bond-Length Alternation. *J. Am. Chem. Soc.* **1994**, *116*, 10703−10714.
(96) Cronstrand, P.; Luo, Y.; Ågren, H. Multi-Photon Absorption of Molecules. *Adv. Quantum Chem.* **2005**, *50*, 1.
(97) Garcia-Vazquez, P.; Morales-Saavedra, O. G.; Pelzl, G.; Banuelos, J. G.; Carreon-Castro, M. P. Incorporation in Langmuir and Langmuir-Blodgett Films of Symmetric Fluorine Substituted Bent-Core Liquid Crystals: Morphological and Optical Properties. *Thin Solid Films* **2009**, *517*, 1770−1777.

https://dx.doi.org/10.1021/acs.jpcc.9b11391
J. Phys. Chem. C 2020, 124, 8310−8322